Nexus : Journal of Innovative Studies of Engineering Science (JISES)
Volume: 02 Issue: 08 | 2023
http://innosci.org/

FATIGUE NATURE OF WELDED A7N01S-T5 ALUMINUM ALLOY AND REACTION TO STRESS CONCENTRATION

SINEBE, Jude Ebieladoh
Mechanical Engineering Department,
Delta State University, Abraka, Delta State, Nigeria
Email: jsinebe@yahoo.com jesinebe@delsu.edu.ng

Annotation: During the welding process, the microstructure and the mechanical characteristics of Aluminum alloys in the heat affected zone of the weld are typically affected. Aluminum alloy plates, (7N01S-T5) having 10milliliters of thickness were welded using metal-inert-gas (MIG) welding technique with ER5356 and ER5087 welding wires. Fatigue strength and tensile strength were examined in this study, as well as the microstructures of the welded joints using electron backscattered diffraction (EBSD) energy dispersion spectroscopy (EDS), and a high frequency fatigue machine among other mechanical properties. To assess the impact of stress concentration, the butt joints reinforcement were evaluated for fatigue strengths. It was determined that the tensile strength as well as the elongation of the 7N01S/5087 welded joint (which consisted of a plate of 7N01S Aluminum alloy that had been welded alongside ER5087 wire) were higher than the 7N01S/5356 welded joint (plate of 7N01S Al. alloy welded with ER5356 wire). The elongation couple with high strength of the 7N01S/5087 welded joint was obviously due to the microstructure being refined in the weld zone. The introduction of Zr element also advances the structure of Al grains around Al3Zr sites. Significantly, the findings demonstrate that the reinforced butt weld had lower fatigue

Key words: ER5087 welding wire; A7N01S-T5; microstructure; ER5356 welding wire; fatigue strength.

Introduction

The 7N01S-T5 Aluminum alloys were commonly employed to various industries as structural materials, and its applications included cryogenic pressure containers and the bodies of high-speed trains (Starke & Staley, 1996). The 7N01S-T5 Aluminum alloy, as a normal Al-Zn-Mg alloy performed well during welding and had exceptional strength with good resistance to corrosion (Deng, Peng, Xu, Pan, Ye, Wang, Lu, & Yin, 2015). Consequently, 7N01S-T5 Aluminum alloy was being employed more and more for the body structures of high-speed trains. The alloy's low weight and great strength have led to its widespread use in China Railway's high-speed trains (Engdahl, Hansen, Warren, & Stiller, 2002). In terms of rating, 90% of structural fractures result from fatigue damage, a common problem associated with joining metal elements by welding (Dong, Li, Sun, Gong, & Liu, 2013). Investigating the fatigue strength of welded joints is therefore important.

Aluminum alloy constructions were typically joined using welding because it may lower the high manufacturing costs and streamline product design (Zhang, Gou, Hang, & Chen, (2017); Pakdil, Çam, Koçak, Erim, (2011) as a result, welding of 7N01S-T5 Aluminum alloy plates has gained much attention recently. Xie, Xiao, Li, Wang, Ma, & Jiang (2019) welded the 7N01S-T5 Aluminum alloy plate by using laser-arc hybrids and ER5356 wire. They discovered that the welded joint indicated less residual stress and outstanding mechanical qualities. In addition, they also noted the fusion zone had the least micro-hardness plus tensile strength, mostly due to the structure of coarse particles and evened grains. Zhang, Wu, Yan, Guo, Chen, & Wang (2014) looked at how the welding heat cycle affected the 7N01S-T5 Aluminum alloy's lifetime and softening characteristics.

The use of metal-inert-gas welding proved to be effective, adaptable and affordable, because of this, it is a common and preferred fusion-welding process for welding of 7N01S-T5 Aluminum alloy in technologically advanced train bodies (Barnes, Raman, Lowerson, & Edwards, 2012; Randić, Pavletić & Turkalj, (2019) and ER5356 wire was used frequently in welding high-speed bodies of trains. Nevertheless, as a result of the granular solidification at the weld zone, the properties of the joined weld with ER5356 wire were not optimum, and also vulnerable to heat cracking (Zaid, Hatab, & Ibrahim, 2011). Thus, the aged ER5356 welding wire must be replaced with a new welding wire. Sadly, not much research has been done on this problem. This study intends to add to the body of knowledge in this field.

It was a wise decision to incorporate rare earth elements into the welding process to enhance properties of the weld joint. By using ER5356 as welding wires added with Sc sample and without Sc sample, Huang, Yin and Lei (2008) performed TIG welding on sheets of 7A52 Aluminum alloy. After adding Sc to ER5356, the yield strength with elongation of the welded joints were 24% and 37% respectively more than just using ER5356 wire alone (Górka, 2020). Though, the amount of wire needed for each carriage to weld the alloy in the train body was quite large (Zhang, Chen, Ma, Zhang, 2018), every carriage weld seam was 2.5 kilometers in length, plus 500 kg of welding wire that was needed. As a result, it was challenging to use the widespread Sc-added welding wire in commercial applications for the purpose of welding the bodies of high-speed trains due to the high production costs. The ER5087 wire, which had Zr added to it was reasonably inexpensive, compatible with base metal and found widespread use in welding of trains. Thus, there was a lot of potential for the ER5087 wire to occupy the current ER5356. **Table 1** below provides summary of literature of Al-Zn-Mg Aluminum alloy weld for easier comprehension.

Table 1. Literature review of Al-Zn-Mg Aluminum alloy weld

Study	Research Contents	Research Findings	Remark
Latest method of welding	ER5356 wire added Laser-arc hybrid	Perfect micro structural characteristics with residual stress	
Analysis of the microstructure matrix for the weld joint	The thermodynamic behaviors of the welded joint	Highest temperature of the thermal cycle that welding process goes through has repercussions on the magnitude and volume of precipitation, which ultimately leads to a softer weld connection.	

Welding wire advancement	In this research, the microstructure and properties of weld joints filled with either ER5356 or Scadded ER5356 weld wires were examined and compared	The incorporation of Sc into the wire allows for successful enhancement of micro-structural properties of the weld join.	Extremely exorbitant price of scadded weld wire prevents its widespread application in commercial settings

For the purpose of this study, welding was performed on a plate composed of Al alloy with ER5087 and ER5356 filler materials in sequential order. A comparison of microstructures and mechanical properties of the joints infused with ER5087 and ER5356 wires were also performed as part of this study. This study came to the conclusion that a new type of wire should be investigated in order to successfully weld the body of a high-speed train that had superior mechanical qualities.

The intensity of the stress is one of the most critical aspects that determines how well joints recover from fatigue (Qingyan Zhu, Lijia Chen, Guangqi Zhu & Xiaoran Huo, 2020) The most significant contributors to stress concentration are discontinuities in the geometric shape of the component and faults in the weld. Butt joints are used in a wide variety of technological applications, and these applications can use reinforced butt joints or perhaps butt joints with no weld reinforcement. When comparing connections without weld reinforcement, we have much less fatigue strength for butt joints to joints that have been weld-reinforced. The impact of stress concentration by weld reinforcement on 7N01S-T5 welded joints has not been well addressed in many previous literatures (Jolu, Le Morgeneyer, Denquin & Gourgues-Lorenzon, 2015). The study evaluated fatigue strengths of the welded joints that had weld reinforcement and those with no reinforcement and calculating the stress concentration factor allowed for it and giving explanation of the outcomes of fatigue testing (Randić, Pavletić,. & Fabić, 2021).

Experimental Methodology

Experimental Materials

The base metal sheet (A7N01S) with a thickness of 10 millimeters was T5 heat-treated earlier before welding (Subjected to cooling from higher temperatures and then naturally aged to ISO 2107:2007 standard). To lessen porosity and also eliminate any form of oxides from the samples before welding, samples were cleaned with chemicals such as ethyl, alcohol, etc. To successfully weld the samples, 1.2 millimeters in diameter of both filler wires were used. Table 2 provides an inventory of the A7N01S alloy with filler wires in terms of their chemical make-ups.

Table 2. A7N01S-T5 chemical make-up with welding wires

	Composition by % weight									
Materials	Zn	Mg	Cu	Mn	Cr	Zr	Ti	Fe	Si	Al
A7N01S	4.25	1.40	0.17	0.31	0.24	0.19	0.10	0.09	0.08	Bal.
ER5356	—	4.95	—	0.02	0.09	—	0.07	—	—	Bal.

ER5087	—	5.01	—	0.9	0.09	0.14	0.11	—	—	Bal.

The Welding Process

The measurements of the alloy plates were 300 millimeters in length, while breadth and the depth of 150 millimeters and 10 millimeters respectively. MIG welding technique was used to weld the plates together. The measurements of the groove are depicted in figure 1 which can be found below. After significant number of welding trials while employing argon shielding gas that was approximately 100% pure, the welding processes were eventually perfected. Before beginning the welding process, ethyl alcohol was used to clean the base metal surface and the welding wires. By using 2 millimeters for the root face to mill a 70-degree angle, the "V-shape" groove was formed. The welding procedure consisted of a total of four layers, and there was a total of six weld beads. **Table 3** presented the various parameters of MIG welding.

Fig.1. Pictorial view of the welding groove

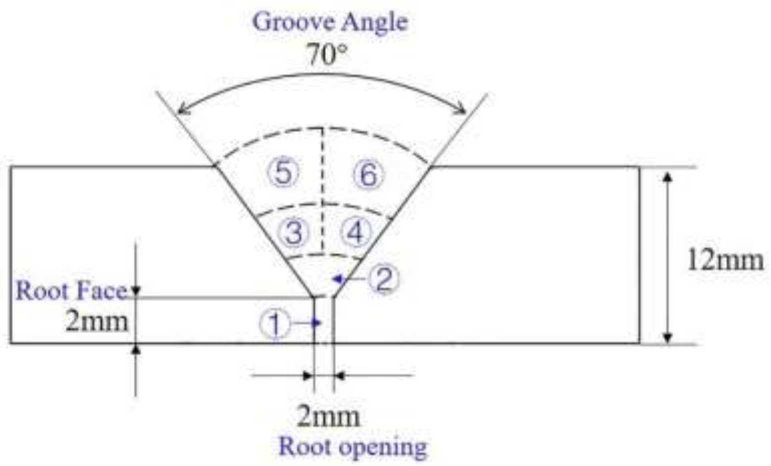

Table 3. MIG welding Specifications

Weld bead No.	Weld technique	Applied Current (Ampere)	Applied Voltage (Voltage)	Flow rate (l/min)	Welding speed (mm/sec)
	Rooting weld	245	23.4	20-25	7.4
3 & 4	Filling weld	261	29.9	20-25	8.0
5 & 6	Capping weld	273	24.1	20-25	8.4

2.3 Mechanical Test and Microstructure Observation

The GB/T 13816-1992 standard was followed for machining fatigue samples. At zero-stress ratio, the tension-tension cyclic load was used for testing the fatigue using electromagnetic resonant high-frequency fatigue machine (MTS-810) in order to replicate the effects on lifetime. Sine wave was used as the waveform for the test. The fatigue limit was determined to be 1×10^7 which was the maximum number of loading cycles that could be performed. Additionally, HVS-1000 digital Vickers micro-hardness tester was also used to conduct measurements of material's Vickers micro-hardness, with the load set at 0.1 kilograms and the dwell duration set at 10 seconds, with intervals of 2 millimeters. Both the bottom and top positions of the cross-sectional area of the 7N01S/5356 welded joints and that of 7N01S/5087 were examined for their integrity. The precise locations of the test lines were depicted in **Figure 3**. The MTS-810 universal testing device was used to conduct tensile testing at room temperature with a tensile velocity of 2 millimeters per minute. All of the data for the test came from three separate but parallel samples. The locations of the tensile specimen samples that were taken for the welding are depicted in **Figure 2**.

Fig.2. Diagrammatic presentation specimen sampling.

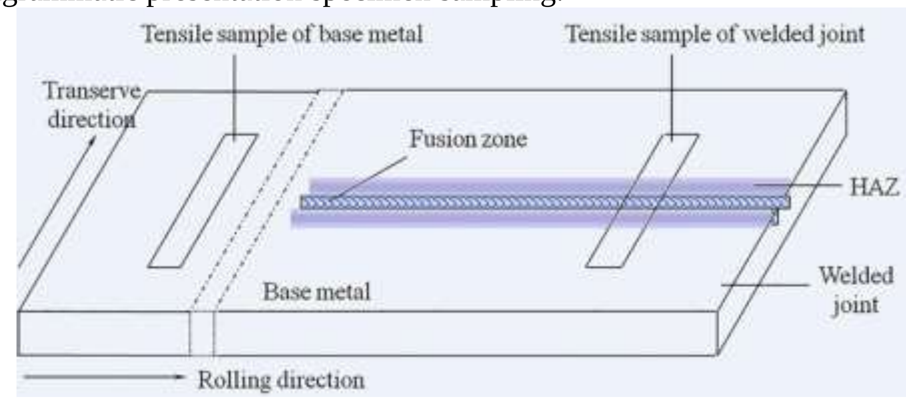

On a Quanta MK2-200 scanning electron microscope, an X-ray Energy Disperse Spectroscopy (EDS) study was done to find out the elemental make-up of the sample (SEM). In order to investigate the grain boundary features present in the various zones of the welded joints, electron backscattered diffraction (also known as Sirion 200) was used.

Fig. 3. Welding joints indicated absolute test lines.

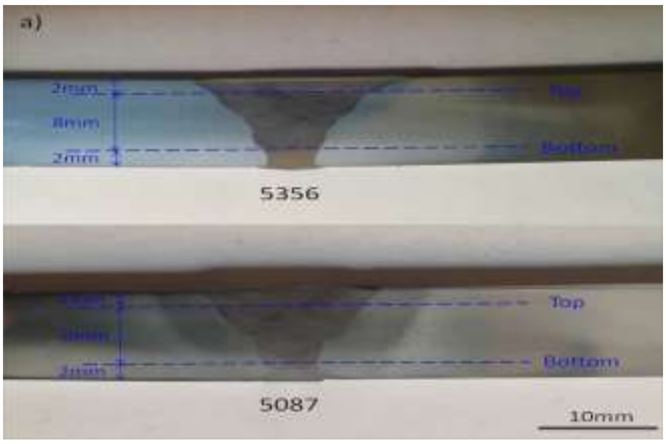

3.0 Findings and Discussion of Results

3.1 The Welded Joints and Distribution of Micro-Hardness

Figure 3 displayed profiles of micro-hardness as well as morphologies cross-sectional area for two welded joints being compared. Both welding wires showed favorable compatibilities with the base metal, 7N01S as evidenced as the joints did not exhibit any macro-level cracks, porosity, or other defects of any kind. For both of the weld, around the welding center line, the distribution of micro-hardness was symmetrical. Weld zone had a minimum value of micro-hardness that was quite low, and the hardness was likewise quite low in the heat affected zone. Both zones were actually affected by the heat when compared side by side. The 7N01/5356 welded junction had a hardness value that ranged from 75-82HV, whereas the ER5087 welding wire-filled welded joint had a hardness value that ranged from 85-95HV.

The Welded Joints and the P–S–N Curves Drawing Technique

In accordance with ISO 12107:2012, curves representing the failure probability as a function of stress amplitude and cycles number were produced. P–S–N curves of several different weld butt joins are depicted in **Figure 4**. Each graphic has two lines and data points that have been measured. The top line of the graph represents P-S-N curve of 50% failure probability with 50% level of confidence, while the bottom line of the graph represents P-S-N curve of 10% probability of failure and 90% confidence level.

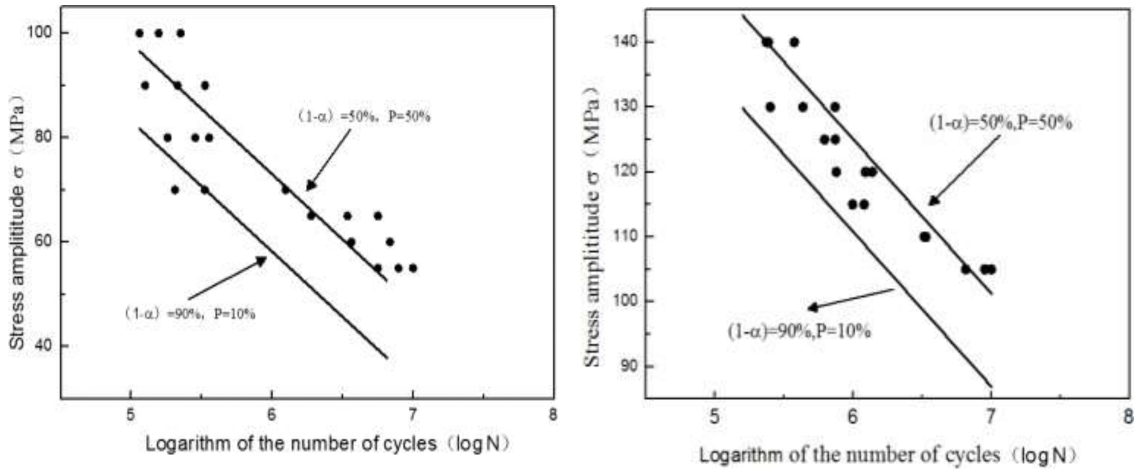

(a) (b)

Fig. 4. Butt joints showing *P–S–N* curves (a) when weld with reinforcement and (b) when weld without reinforcement.

The fatigue strength for the butt reinforced weld is 52.33 MPa for 50% failure probability and 50% confidence, compared to 37.5 MPa of 10% failure probability with 90% level of confidence. Both values can be found by using the notation y(50,50). When weld reinforcement is not present in butt joints, the value of y(50,50) is 103.75 MPa, while the value of y(10,90) is 89.47 MPa. Clearly, the butt joint fatigue limit with weld reinforcement is approximately 50% less than that of joints that do not have the weld reinforcement. When compared to joints with no weld reinforcement, a reinforced butt weld has fatigue limit that is significantly lower. The variation in fatigue strengths of these joints gets increasingly remarkable as both confidence and failure probability increases. The morphologies of fracture for the fatigued samples were investigated in order to explain the previously mentioned phenomena and investigate the factors that led to the breaking.

3.3 Weld Fracture and the Mechanism

3.3.1 Morphologies of Fractures in Samples Containing Weld Reinforcement

The figures below indicate fracture morphologies of samples with weld reinforcement

Fig. 5 Fracture morphologies of reinforced weld sample

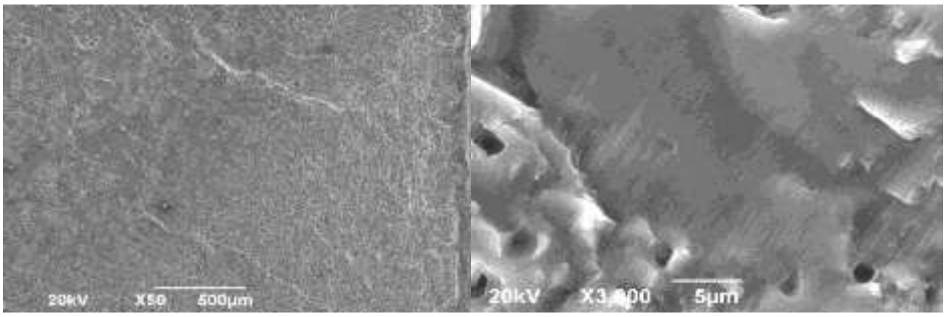

(a) (b)

Fig. 6 Fracture images of reinforced weld joint: (a) crack starting point (b) crack expansion area.

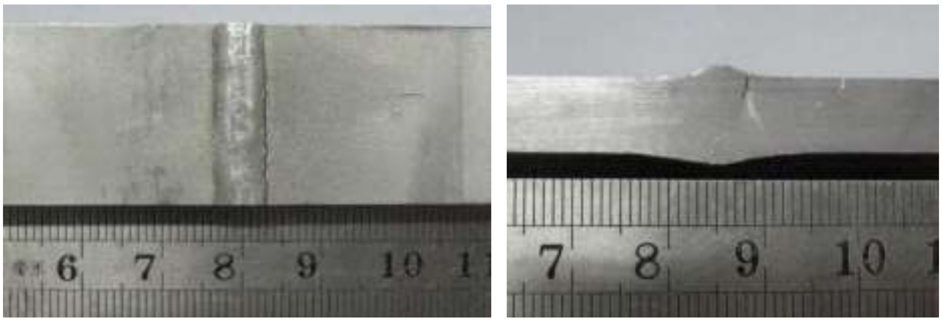

(a) (b)

Fig. 7 Appearance of a broken sample with the weld reinforcement: (a) the weld root and (b) profile of the joint.

Figure 6 illustrates how fatigue crack began close to the weld's root edge (a). The origin of the crack has a line-like morphology because of stress concentration that is caused by weld reinforcement. The form of the firm crack propagation zone is displayed in Figure 6(b). Figure 6 provides an excellent illustration of fatigue striations (b). **Figure 7** reveals what appears to be a damaged sample. We can infer that the weld root is where the fatigue crack started.

3.3.2 Morphologies Fracture of Samples without Reinforcement Weld

The fracture morphologies of a fractured sample that do not have the weld reinforcement are depicted in **Figure 8**. The surface porosity was the source of the cracking, as seen in **Figure 8**. (a). Clearly visible fatigue striations can be seen in the area depicted in **Fig. 8** (b), which depicts the area of stable fracture propagation. Porosity on the surface of the specimens enables them to produce stress concentration as a result fatigue fracture.

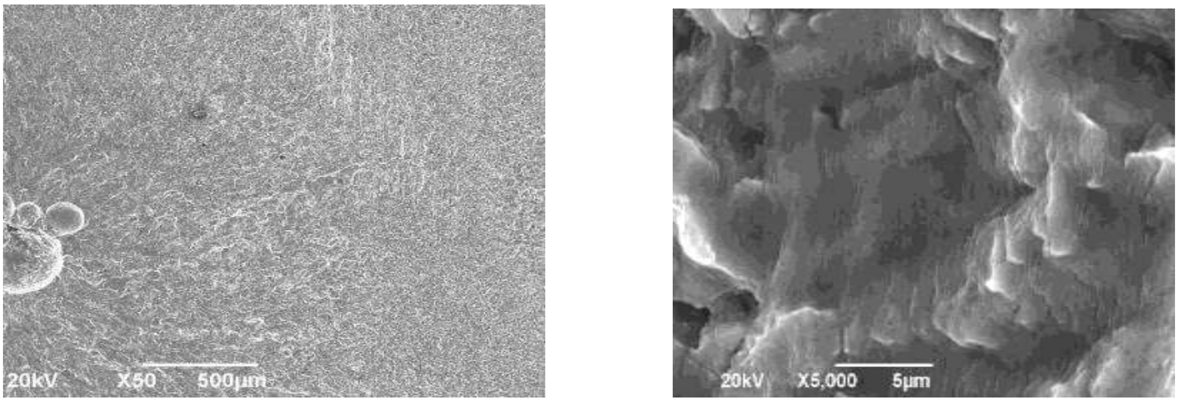

(a) (b)

Fig. 8. SEM pictures of the fracture joint with no reinforcement (a) starting wear point (b) extended fatigue

3.4 The Weld Tensile Strength

Figure 9 displays the tensile characteristics of the welded joints that were created with ER5087 and ER5356 as filler materials. The weld zone was where any fractures that occurred in any of the specimens could be found. The 7N01/5087 welded joint had an ultimate strength, yield strength and elongation corresponding to 320 MPa, 186 MPa and 6.4% respectively, compared to 288 MPa, 176 MPa, and 4.9% for the 7N01/5356 welded joint. Additionally, the mean strength with the elongation of 7N01/5087 joint appeared higher than those of the 7N01/5356 welded joint.

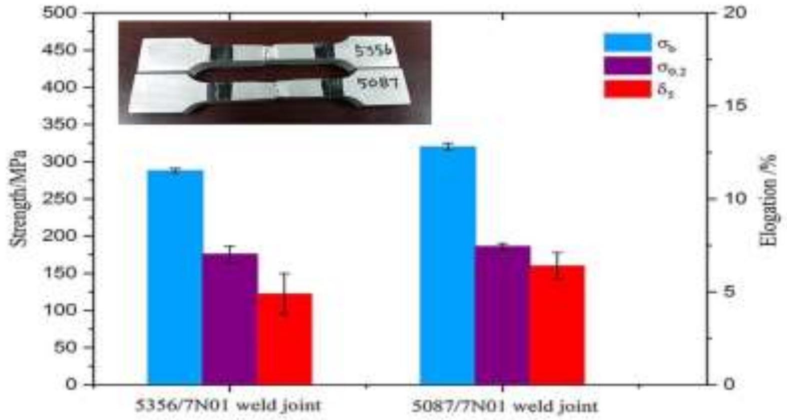

Fig. 9 Welded joints depicting tensile properties

3.5 The Microstructures of Welded Joints with EBSD images

EBSD pictures of the joints and base material are displayed in **Figure 10**. Fusion Zone (FZ), base material (BM), the Heat-Affected Zone (HAZ) and the Weld Zone (WZ) are four separate zones that make up the microstructure of MIG welded joints. Microscopically, the base metal microstructure was fibrous and extended in the direction of rolling; it also contained a negligible rate of grain recrystallization (**Fig. 10**a). In contrast to the 7N01/5087 weld zone, which had grain sizes that were roughly 5-25µm, the seizes of grains of the 7N01/5356 weld zone were integrated within the range of 30-65µm (**Fig. 10**d and e) (**Fig. 10**b and c). Fusion and the weld zones had strong bonds, and the weld zone's microstructure consisted of coarse columnar crystals (**Fig. 10**f and g). Images of the two welded joints are shown in **Figure 10** a, base metal, weld zone, grain size distribution image of the weld zone, fusion zone and representation of the color code used to identify the crystallographic orientations on standard stereographic projection. The welded joint 7N01/5356 d), the weld zone, e and a picture of the grain size distribution (red, blue and green) are indicated.

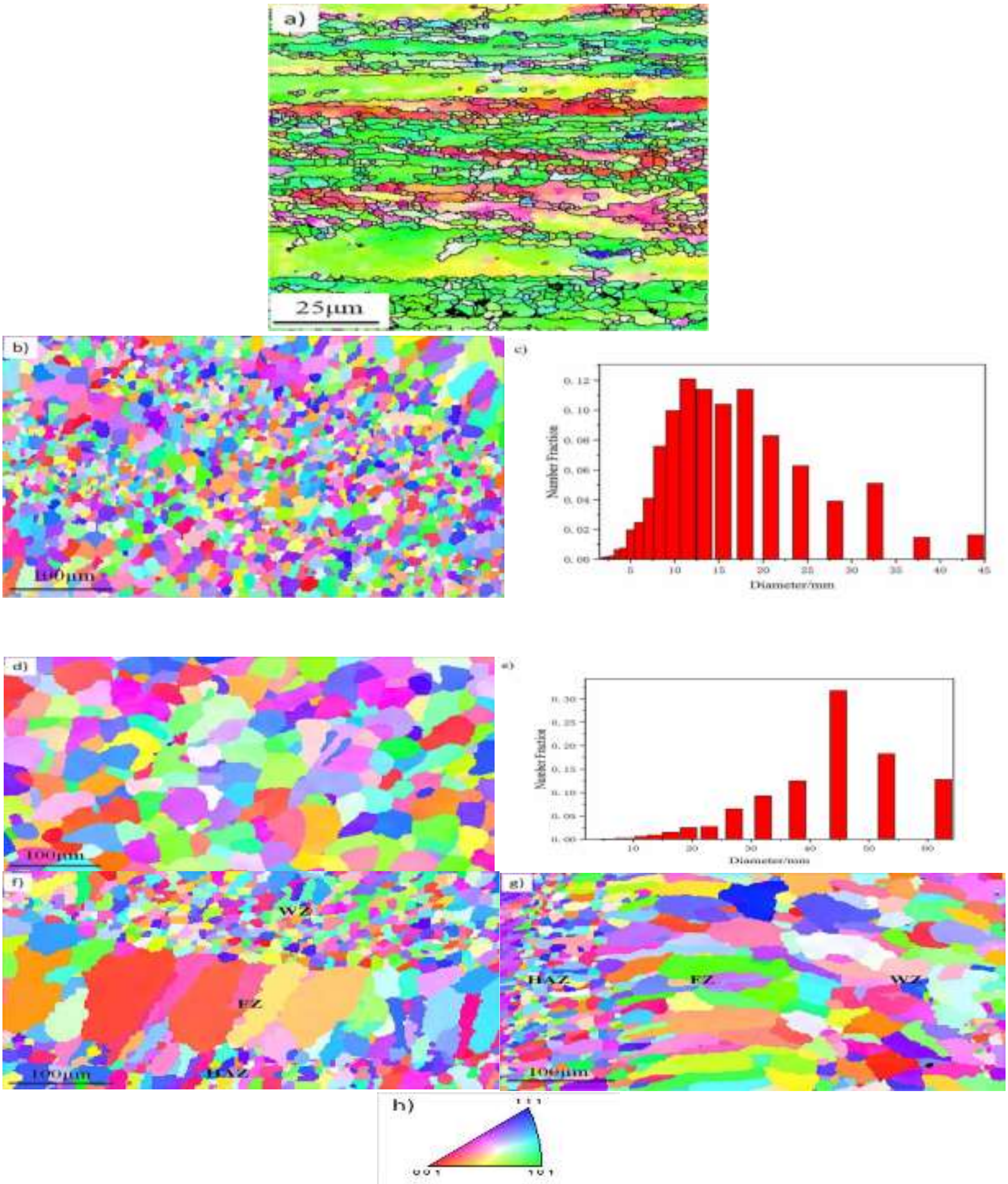

3.6 The Welded Joints and Energy Disperse Spectroscopy (EDS)

The findings of the EDS analysis of the two weld joints were displayed in **Figure 11**. The constituents that made up the 7N01/5087 weld zone were, for the most part, identical to those that made up the ER5087 wire. Additionally, the weld zone, 7N01/5087 contained Zr and Mn elements with higher concentration of Mn element to that of the weld zone 7N01/5356 (Fig. 11c and d).

Fig. 11 The following are the findings of EDS on the zones: a, c and b, d represents 7N01/5356 and 7N01/5087 welded joint respectively.

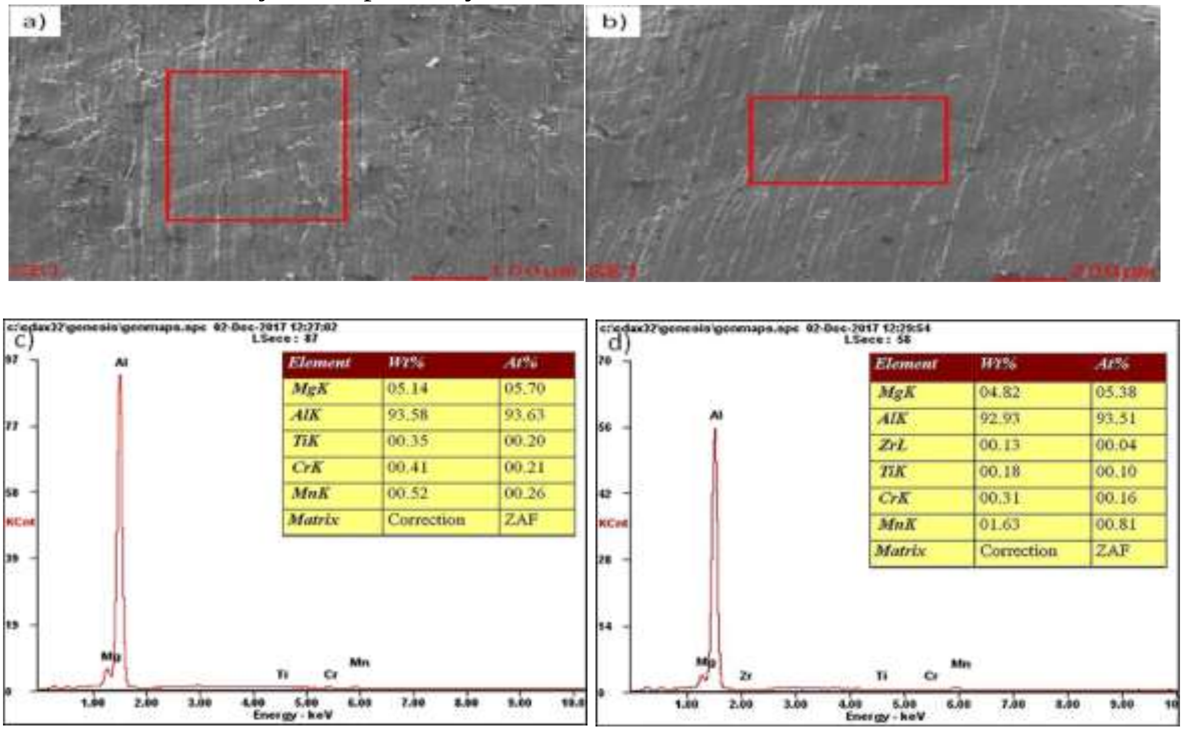

3.7 Welded Joints and Factor of Stress Concentration

The above-mentioned facts allow for the inference of two different conclusions: (1) The most important factor in fatigue fracture is stress concentration, which can be brought on by either weld reinforcement or weld flaws. (2) The stress concentration that is the outcome of weld reinforcement has a greater impact than the stress concentration which is the consequence of weld flaws. The stress concentration factor brought on by the welded reinforcement was calculated in order to conduct a quantitative examination of the phenomena. A schematic picture of a reinforced butt weld is revealed in **Fig. 12**. In this diagram, ***B*** stands for the weld's width, **h** for the weld reinforcement's height, for the weld's transition angle, ***t*** for the plate's thickness, and ***r*** for the weld's transition radius on the welding side. **Table 4** displays the findings of the measurements and computations made after six samples were analyzed.

Table 4. Butt weld measurement with reinforcement

Dimension and Description	*B*	*h*	***θ***	*t*	*r*
Values (mm)	5.29	1.19	1.69	7.9	5.09

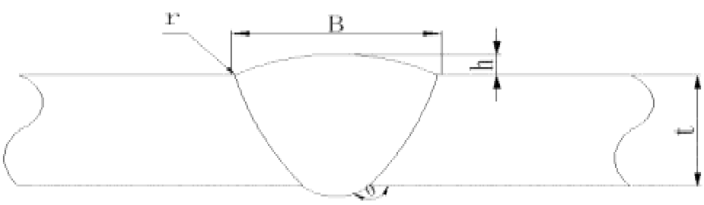

Fig. 13. Diagram of reinforced butt weld

From **Refs.** 30–32, the factor of stress concentration K_T can be deduced as:

$$K_T = \{1 + f(\theta)\,[g(r) - 1]\}\, C(a/t), \quad (1)$$

The zones experiencing incomplete penetration and their length is denoted as **a**; whereas $f(\theta)$, $g(r)$ as well as $C(a/t)$ are related coefficients to θ, r and (a/t) respectively. Thus, it can be estimated by Eqs. (2) - {(4) in the following fashion:

$$f(\theta) = \frac{1 - exp\left\{-0.9\sqrt{\frac{\omega}{2h}}\,(\pi - \theta)\right\}}{1 - exp\left\{-0.9\sqrt{\frac{\omega}{2h}}\,(\frac{\pi}{2})\right\}}, \quad (2)$$

$$g(r) = a_t g_t(\mathrm{r}) + a_b g_b(\mathrm{r}), \quad (3)$$

$$C(a/t) = 1 + 0.64\,\frac{(^a/_t)^2}{2hr/t} - 0.12\,\frac{(^a/_t)^4}{(2hr/t)^2}, \quad (4)$$

here **ω** is regarded as similar length with respect to the type of joint. Like butt weld type, **ω** we can calculate by Eq. (5):

$$\omega = t + 2h + 0.6B. \quad (5)$$

From Eq. (3), variables, a_t and a_b are functions related to the type of load. This is so since tensile loads only were used in this examination. Also, a_t had the numerical vale of **1**, while a_b was noted to be **0**. On the other hand, the bending load is related to variable, $g_t(\mathrm{r})$; and so therefore, its value in this study is zero.

The tensile load is related to the variable, $g_t(\mathrm{r})$ and we can calculate it as:

$$g_t(\mathrm{r}) = 1 + \beta_t\,[(h/r)\frac{1}{2.8(\frac{\omega}{t}) - 2}]^{0.65} \quad (6)$$

For a butt weld, β_t = 2:0.

For this study, X-rays were used to inspect the specimens used with no defects indicating incomplete penetration; hence, for $C(a/t)$, the value was 1. From the values in **Table 4**, with the earlier equations, K_T can be calculated; and this is equal to 1.50. This implies that the maximum stress is 1.5 times than the average stress. The weld root becomes the weakest section when subjected to cyclic stress because the stress concentration brought on by the weld reinforcement is of such a severe nature. This results in a significant reduction in the fatigue strength of butt joints that have weld reinforcement.

4.0 Conclusions

In conclusion, the 7N01T5 Aluminum alloy plates were welded using welding wires ER5356 and ER5087, and then a relative investigation of the mechanical characteristics with microstructures of the connected joints was carried out. The following are some of the deductions that can be derived from the outcomes of the experiment:

- When compared to the A7N01/5356 welded sample, the joints that were welded using ER5087 weld wire had superior mechanical properties. The ultimate strength and elongation of the A7N01/5087 welded joint was 320 MPa and 6.4%, respectively, while those of the A7N01/5356 welded joint was 288 MPa and 4.9%, respectively
- The high strength, good elongation of the A7N01/5087 welded joints were mostly ascribed to the microstructure refinement that took place in the weld zone as a result of the addition of Zr element, which promoted the nucleation of Al grains around Al3Zr sites
- In joints that have weld reinforcement, cracks of fatigue emerged from the weld root as a result of load concentration. On the other hand, fatigue cracks in joints with no reinforcement come from welding flaws such as pores
- Fatigue limit of weld that have been reinforced is significantly lower than the fatigue limit of joints that do not have weld reinforcement
- The weld reinforcement increases the stress concentration factor of joints by 1.5. The fatigue strength decreases as a result of the excessive stress concentration.

Reference:

1. Barnes, A. J., Raman, H., Lowerson, A., & Edwards, D. (2012). Recent Application of Superformed 5083 Aluminum Alloy in the Aerospace Industry. *Materials Science Forum*, *735*, 361–371. https://doi.org/10.4028/www.scientific.net/msf.735.361
2. Deng, Y., Peng, B., Xu, G., Pan, Q., Ye, R., Wang, Y., Lu, L. & Yin, Z. (2015). Stress corrosion cracking of a high-strength friction-stir-welded joint of an Al–Zn–Mg–Zr alloy containing 0.25wt.% Sc, *Corrosion Science*, *100*, 57-72. ISSN 0010-938X, https://doi.org/10.1016/j.corsci.2015.06.031.
3. Dong, P., Li, H., Sun, D., Gong, W, & Liu, J. (2013). Effects of welding speed on the microstructure and hardness in friction stir welding joints of 6005A-T6 aluminum alloy, *Materials & Design*, *45*, 524-531,ISSN 0261-3069,https://doi.org/10.1016/j.matdes.2012.09.040.
4. Engdahl, T., Hansen, V., Warren, P.J. & Stiller K. (2002). Investigation of fine scale precipitates in Al–Zn–Mg alloys after various heat treatments, Materials Science and Engineering: A, 327 (1), 59-64, ISSN 0921-5093, https://doi.org/10.1016/S0921-5093(01)01876-7
5. Górka, J. (2020). The assessment of the quality of welded joints made of abrasion-resistant plates using the nanocrystalline filler metal. *Journal of Mining and Metallurgy, Section B: Metallurgy*, *56*(2), 209-220. Retrieved from https://aseestant.ceon.rs/index.php/jmm/article/view/21717
6. Huang, J., Yin, Z. & Lei, X. (2008). Microstructure and properties of 7A52 Al alloy welded joint, Transactions of Nonferrous *Metals Society of China*, *18*, (4), 804-808, ISSN 1003-6326. https://doi.org/10.1016/S1003-6326(08)60139-9.

7. Jolu, T., Le Morgeneyer, T.F., Denquin, A. & Gourgues-Lorenzon, A.F. (2015). Fatigue lifetime and tearing resistance of AA2198 Al–Cu–Li alloy friction stir welds: Effect of defects, *International Journal of Fatigue, 70,* 463-472, ISSN 0142-1123,. https://doi.org/10.1016/j.ijfatigue.2014.07.001.
8. Kang Zhang, J.Q. Chen, P.Z. Ma, X.H. Zhang, (2018). Effect of welding thermal cycle on microstructural evolution of Al–Zn–Mg–Cu alloy, *Materials Science and Engineering: A, 717.* 85-94, ISSN 0921-5093. https://doi.org/10.1016/j.msea.2018.01.067.
9. Pakdil, M. Çam, G. Koçak, M. Erim, S. (2011). Microstructural and mechanical characterization of laser beam welded AA6056 Al-alloy, *Materials Science and Engineering: A, 528,* (24), 7350-7356, ISSN 0921-5093, https://doi.org/10.1016/j.msea.2011.06.010.
10. Randić, M., Pavletić, D. & Turkalj, G. (2019). Multiparametric investigation of welding techniques on toe radius of high strength steel at low-temperature levels using 3D-scanning techniques. Metals , 9, 1355.
11. Qingyan Zhu, Lijia Chen, Guangqi Zhu & Xiaoran Huo (2020). Hysteresis energy based low cycle fatigue properties analysis in extruded Al-7Zn-2Mg-1.5Cu-0.2Sc-0.1Zr alloy at low temperature. *Materials Research Express*, *Volume 6*, (11). **DOI** 10.1088/2053-1591/ab4ab8
12. Randić, M., Pavletić, D. & Fabić, M. (2021). Evaluation of the Stress Concentration Factor in Butt Welded Joints: A Comparative Study. *Metals 11*(3),411; https://doi.org/10.3390/met11030411
13. Starke, E.A. Staley, J.T. (1996). Application of modern aluminum alloys to aircraft, Progress in Aerospace Sciences, 32, (2–3), Pages 131-172, ISSN 0376-0421, https://doi.org/10.1016/0376-0421(95)00004-6
14. Xie, H., Xiao, Z., Li, Z., Wang, M., Ma, S & Jiang, H. (2019). Quench sensitivity of AA7N01 alloy used for high-speed train body structure. *JOM: the journal of the Minerals, Metals & Materials Society* *71*(5). DOI: 10.1007/s11837-018-3162-z
15. Zaid, H.R., Hatab, A.M. & Ibrahim, A.M.A. (2011). Properties enhancement of alzn-mg alloy by retrogression and re-aging heat treatment. *Journal of Mining and Metallurgy Section B Metallurgy* *47* (1) B 31 – 35.
16. Zhang, M., Gou, G., Hang, Z. & Chen, H. (2017). Effect of stress concentration on the fatigue strength of A7N01S-T5 welded joints. International Journal of Modern Physics B .31 (16-19), 1744047
17. Zhang, H.X. Wu, G.H. Yan, Z.F. Guo, S.F. Chen, P.D. & Wang, W.X (2014). An experimental analysis of fatigue behavior of AZ31B magnesium alloy welded joint based on infrared thermography, *Materials & Design*, *55*,785-791, ISSN 0261-3069. https://doi.org/10.1016/j.matdes.2013.10.036.